Journal of Power Sources 217 (2012) 229–235

Contents lists available at SciVerse ScienceDirect

Journal of Power Sources

journal homepage: www.elsevier.com/locate/jpowsour

FeS_2/C composite as an anode for lithium ion batteries with enhanced reversible capacity

D. Zhang [a], Y.J. Mai [a], J.Y. Xiang [b], X.H. Xia [a], Y.Q. Qiao [a], J.P. Tu [a,*]

[a] State Key Laboratory of Silicon Materials and Department of Materials Science and Engineering, Zhejiang University, Hangzhou 310027, China
[b] Narada Power Source Co., Ltd, Hangzhou 311305, China

HIGHLIGHTS

- FeS_2/C composite is prepared by a simple solid state reaction for the first time.
- The result of XPS shows the carbon coating can reduce the corrosion from HF.
- The result of ICP shows the carbon coating can reduce the dissolution of sulfur.
- FeS_2/C composite shows superior electrochemical performance.

ARTICLE INFO

Article history:
Received 26 February 2012
Received in revised form
23 May 2012
Accepted 29 May 2012
Available online 19 June 2012

Keywords:
Iron disulfide
Carbon coating
Cycle performance
Lithium ion battery

ABSTRACT

Carbon coated FeS_2 (FeS_2/C) composite is prepared via a simple solid state reaction using glucose as carbon source. The porous FeS_2 particles are uniformly surrounded by the amorphous carbon coating. As an anode material for lithium ion batteries, the FeS_2/C composite exhibits higher reversible capacity and better cycling performance than the unmodified FeS_2. The specific capacity of the FeS_2/C composite after 50 cycles is 495 mAh g^{-1}, much higher than that of FeS_2 (345 mAh g^{-1}). In order to investigate the effect of carbon coating, the cycled electrodes have been analyzed by X-ray diffraction (XRD), scanning electron microscopy (SEM) and X-ray photoelectron spectroscopy (XPS). The improvement is attributed to the introduction of carbon coating, which can enhance the conductivity, reduce the dissolution of sulfur and corrosion from HF, and stabilize the porous structure during cycling.

1. Introduction

Iron disulfide (FeS_2) is an attractive anode material for lithium ion batteries (LIBs) because of its interesting characteristics such as high theoretic capacity (890 mAh g^{-1}), low environmental impact and affordable cost [1–3]. However, its practical application is restrained by the poor cycling stability resulting from the poor electrical conductivity and the cycleability of sulfur, causing deterioration of active materials during cycling [3]. A variety of appealing strategies have been utilized to solve these intractable problems. For example, Montoro et al. found that the gelatin-pyrite composite electrode could sustain 279 mAh g^{-1} after 15 cycles in the voltage range of 1.1–3.2 V (vs. Li/Li^+) at 0.4 mA cm^{-2} [4]. Choi et al. reported a nickel-precipitated pyrite which could exhibit an initial discharge capacity of 600 mAh g^{-1} at 89 mA g^{-1} between 0.8 and 2.4 V (vs. Li/Li^+) [5]. However, it is still a great challenge to obtain high-performance FeS_2 electrode material with both large reversible capacity and long cycling life.

Composite with carbon is expected to be an advanced anode material in LIBs [6–17]. It is reported that the carbon coating can suppress the aggregation of active particles and the side reactions between the active material and electrolyte, increasing their structure stability during cycling [18]. Besides, the carbon can enhance the electrical contact among the active materials, in principle, are easier to bind than isolated nano-sized particles [9,19–22]. What is more, the carbon coating could also act as elastic buffers to relieve the strain associated with the volume change during lithium insertion/extraction [23].

Although carbon coating is widely used in the investigation of many materials such as NiO, SnO_2 anode materials, there are few reports dedicated to FeS_2/C composite [24,25]. In this present work, carbon coated FeS_2 composite is prepared by a simple solid state reaction. The electrochemical properties of the FeS_2/C composite and FeS_2 electrodes are investigated. As a result, preliminary

* Corresponding author. Tel.: +86 571 87952856; fax: +86 571 87952573.
E-mail addresses: tujp@zju.edu.cn, tujplab@zju.edu.cn (J.P. Tu).

0378-7753/$ – see front matter © 2012 Elsevier B.V. All rights reserved.
http://dx.doi.org/10.1016/j.jpowsour.2012.05.112

experiments in this study show that the as-prepared FeS_2/C exhibits excellent electrochemical performance with high capacity retention and specific capacity during cycling. Furthermore, the reasons for the improvement on the electrochemical properties are discussed in detail through many measurements, especially XPS.

2. Experimental

FeS_2/C powder was prepared by a simple solid state reaction. Firstly, a mixture of $FeC_2O_4 \cdot 2H_2O$, S powder and glucose with a molar ratio of 1:3:0.12 was dispersed in alcohol and planetary milled for 8 h at a rotating speed of 350 rpm. Ball-milling was carried out at room temperature in air using agate vial and balls (ball/powder weight ratio of 8:1). Then, the as-prepared precursor was dried in an oven at 60 °C. After alcohol was completely removed, the precursor was placed in porcelain boats, and then calcined at 380 °C for 2 h under Ar flow in a tube furnace to get crystallized FeS_2/C. The FeS_2 powder was prepared without glucose in the same way for comparison.

The crystal structure and morphology of FeS_2 and FeS_2/C composite were investigated by X-ray diffraction (XRD, D/Max-2550), field emission scanning electron microscopy (FESEM, FEI SIRION) and transmission electron microscopy (TEM, JEOL JEM200CX). As the electrode after cycles is sensitive to atmospheric moisture, sample preparation for XRD was carried out in the glove box. In addition, the surface of cycled electrodes was covered with a layer of poly(vinyl chloride) (PVC) film in order to minimize exposure of electrode to atmospheric moisture during data acquisition. The weight content of C in the FeS_2/C composite was tested by Element Analyzer (Flash EA 1112). The specific surface areas of the samples were measured following the multipoint Brunauer–Emmett–Teller (BET) procedure from the N_2 adsorption–desorption isotherms. N_2 adsorption–desorption isotherms were collected at liquid nitrogen temperature using an AUTOSORB-1-C gas sorption analyzer. DSC–TGA analysis of the precursor was measured on a SDT Q600 apparatus in the temperature range of 28–600 °C at a heating rate of 10 °C min^{-1} under an Ar flow of 120 ml min^{-1}. The content of the S content in cycled electrolyte was analyzed by inductive coupled plasma spectrometry (IRIS Intrepid II XSP). XPS analysis was conducted using X-ray photoelectron spectroscopy (Kratos AXIS Ultra DLD) and the vacuity is better than 6.8×10^{-9} Pa during the data acquisition. The electrodes for XPS analysis were obtained from the coin-type cells charged to 2.6 V and transferred to the inert sample transporter with 4-way cross in the glove box.

Electrochemical performances were performed by assembling CR2025 coin cells. To prepare electrodes, the FeS_2 or FeS_2/C (60 wt. %) was homogeneously mixed with acetylene black (25 wt. %) as conducting agent and PVDF as binder (15 wt. %). Firstly, PVDF was dissolved in N-methyl-pyrrolidone (NMP). Then the mixture of acetylene black and FeS_2 powder was milled for 30 min and mixed with PVDF by mechanical agitation for 3 h. The slurry was spread uniformly on aluminum foil at room temperature. After dried at 100 °C for 12 h, the composite film was pressed under a pressure of 10 MPa. The cells were assembled under high pure argon atmosphere in a glove box using FeS_2 electrode as the working electrode, metallic lithium foil as the counter electrode, 1 M $LiPF_6$ in ethylene carbonate (EC)-dimethyl carbonate (DMC) (1:1 in volume) as the electrolyte and a polypropylene micro-porous film (Cellgard 2300) as the separator.

The galvanostatic charge–discharge tests were conducted on LAND battery program-control test system at rates of 0.05–0.2 C (1 C = 890 mA g^{-1}) between 1.2 and 2.6 V at room temperature. CV and EIS measurements were carried out on CHI 660C electrochemical workstation. CV tests were recorded at a scan rate of 0.1 mV s^{-1} from 1.1 to 2.7 V (versus Li/Li^+). EIS tests were performed using a three-electrode cell with the as-prepared FeS_2 as the working electrode, metallic lithium foil as both the counter and reference electrodes, over a frequency range of 100 kHz to 10 mHz under AC stimulus with 5 mV of amplitude and no applied voltage bias.

3. Results and discussion

The DSC–TGA curves of the precursor for FeS_2/C are shown in Fig. 1. The TGA curve shows four main steps of weight loss over the temperature range. The peak at around 100 °C in DSC curve can be assigned to the loss of absorption water of the mixture and the melting of sulfur. The weight loss from 150 to 230 °C in TG curve is related to the thermal decomposition of glucose and the decomposition of FeC_2O_4. The endothermic peak at 300 °C can be attributed to the formation of FeS_2/C composite. In the range of 300–380 °C, the FeS_2/C is stable [26]. It has been previously reported that the glucose can be carbonized to amorphous carbon at about 380 °C [11,27]. Above 380 °C, the weight loss turns evident again, which is associated with the decomposition of FeS_2. Therefore, FeS_2/C composite is prepared at 380 °C.

Fig. 2 shows the XRD patterns of FeS_2 and FeS_2/C powders. The diffraction peaks of both samples are similar and can be perfectly identified as a single phase of pyrite FeS_2 (JCPDS card No. 42-1340) with a cubic structure indexed to Pa3 [205] space group. The content of carbon in the composite is calculated to be 5.34 wt. % tested by an element analyzer. However, no peak of carbon is observed in XRD pattern, thus it is concluded that the carbon is amorphous.

The morphology and detailed structure of samples are illustrated by SEM and TEM images. Fig. 3a shows that the FeS_2 particles are composed of rod-like second particles with diameters of 0.2–1 μm and lengths of 0.5–3 μm. And the rod-like second particles are made up of small first nanoparticles with 30–100 nm in diameters. The pores between the nanoparticles are 5–30 nm in size (Fig. 3b). For the FeS_2/C particles, the porous structure and the particle size is still maintained, indicating that the introduction of carbon does not influence the morphology (Fig. 3c,d).

A typical TEM image of the unmodified FeS_2 particle confirms the porous structure (Fig. 4a). The regularity of the lattice image reveals the crystallinity of these particles (Fig. 4b). The space between the adjacent planes is 2.7 Å, which corresponds well to the (200) plane of FeS_2. After coating with carbon, this nanoporous structure is preserved (Fig. 4c), which is consistent with the SEM

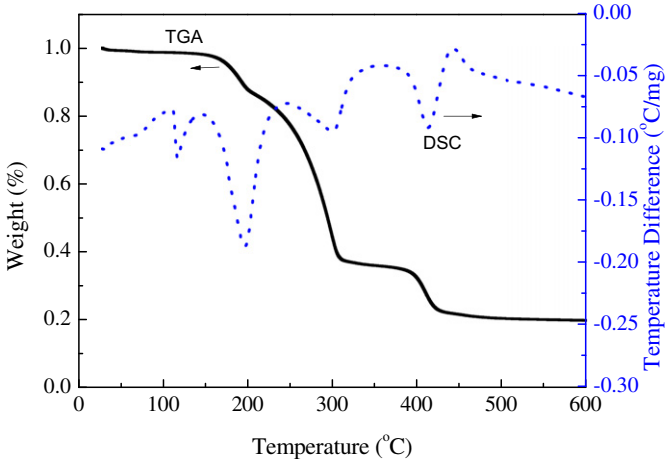

Fig. 1. DSC–TGA curves of the precursor for FeS_2/C recorded from 28 °C to 600 °C with a heating rate of 10 °C min^{-1} under an Ar flow of 120 ml min^{-1}.

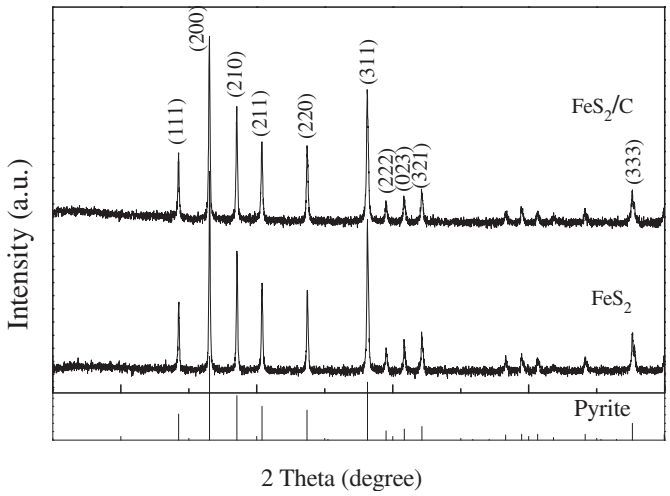

Fig. 2. XRD patterns of FeS_2 and FeS_2/C powders.

image. The surface of the FeS_2 particle is coated by an amorphous carbon layer with 1.0–3.0 nm in thickness (Fig. 4d). The FeS_2/C composite exhibits smaller surface area (14.57 $m^2\ g^{-1}$) than that of the FeS_2 (18.32 $m^2\ g^{-1}$) from the result of BET. It may be due to that some pores between the first nanoparticles are filled by the carbon, leading to reduced specific surface area. The FeS_2/C composite particles also show regular lattice image and the space between the adjacent planes corresponds well to the (200) plane of FeS_2 (Fig. 4d).

Fig. 5 shows the first two discharge–charge curves of the porous FeS_2 and FeS_2/C electrodes between 1.2 and 2.6 V at 0.05 C. The first discharge/charge voltage profiles as well as the second cycle for the FeS_2 and FeS_2/C electrodes are very similar. Both the electrodes exhibit initial discharge plateau at around 1.5 V corresponding to the transformation from FeS_2 to Li_2S and Fe, and two charge plateaus at near 1.8 and 2.45 V indexed to the formation of Li_2FeS_2, Li and further to FeS_y, S and Li [4,28]. Besides, the second discharge curves show an additional discharge plateau at about 2.0 V, suggesting a change in the mechanism of pyrite reduction. It is considered that the Li^+ intercalation/extraction potential of carbon is low (<0.5 V) and the content of carbon is small, thus the capacity contribution of carbon can be neglected. The FeS_2 electrode delivers an initial discharge capacity of 840 mAh g^{-1}, thus the lithium concentration transferred to the pyrite electrode reaches about 3.78e/FeS_2. The FeS_2/C composite electrode delivers an initial discharge capacity of 784 mAh g^{-1}. The lower discharge capacity of FeS_2/C should be attributed to its small contact area with electrolyte, resulting in limited sites to accommodate Li^+. The similar behaviors are also reported for other carbon-coating materials, such as $LiNi_{1/3}Mn_{1/3}Co_{1/3}O_2$–C [29] and NiO–C [9].

Fig. 6 shows the cycling performance of the two electrodes at 0.05 and 0.2 C, respectively. The specific reversible capacity of FeS_2/C composite after 50 cycles is 495 mAh g^{-1} at 0.05 C and 371 mAh g^{-1} at 0.2 C, respectively, much higher than those of FeS_2 (345 mAh g^{-1} at 0.05 C and 237 mAh g^{-1} at 0.2 C). In addition, the FeS_2/C composite exhibits better capacity retention. After 50 cycles, the FeS_2/C composite could sustain 79.3% and 68.9% capacity of the 2nd cycle at 0.05 and 0.2 C, respectively, compared with 55.3% and 42.7% for FeS_2. As can be seen, the introduction of carbon coating results in the improved cyclability of FeS_2.

XPS is a useful measure to investigate the surface of electrodes and the XPS spectra of F 1s of the cycled electrodes are shown in Fig. 7 [1,30–37]. Three types of fluoride which correspond to fluoride atoms in different functional groups appear clearly. The product is determined by the binding energy and kinetic energy for F 1s. According to the Auger spectrum (655 eV), these peaks of binding energies correspond to LiF (685 eV), Li_xPF_y (687 eV) and PVDF (687.8 eV) [38]. Li_xPF_y is the oxidation state of $LiPF_6$ [38]. The hydrolysis of the dominant lithium salt $LiPF_6$ in electrolyte produces HF, LiF and POF_3. It is supposed that the formation of LiF is also attributed to the reaction of POF_3 with Li_2S, HF with Li_2S, and HF with the intermediate product Li_2FeS_2 [39,40].

It is clearly seen that there is a significant difference between the FeS_2/C and FeS_2 electrodes in the range of 685–688 eV. The content of PVDF is identical, but the intensity of PVDF displayed in the FeS_2 electrode is much lower than that of the FeS_2/C, being due to the small detection range of XPS and the large proportion of LiF

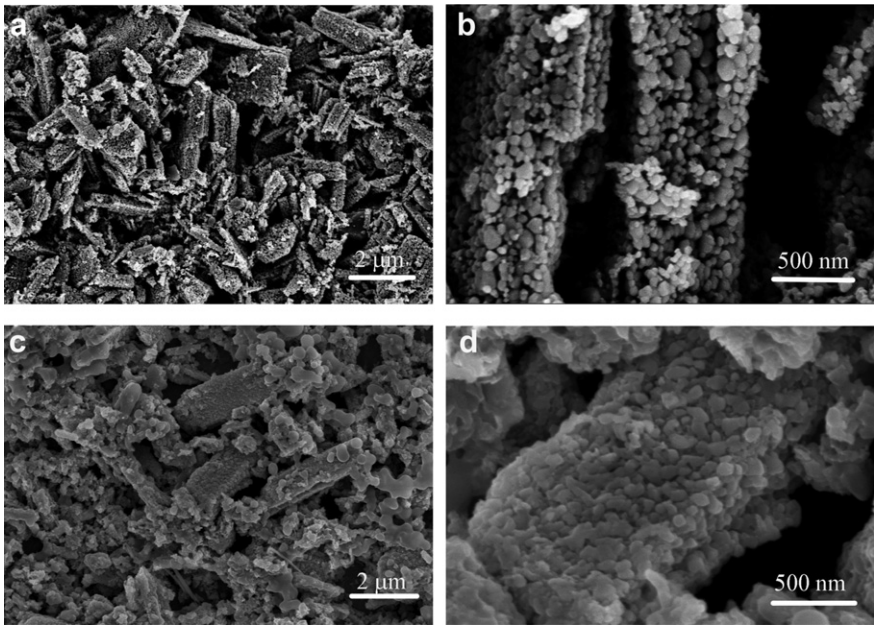

Fig. 3. SEM images of (a, b) FeS_2 and (c, d) FeS_2/C powders.

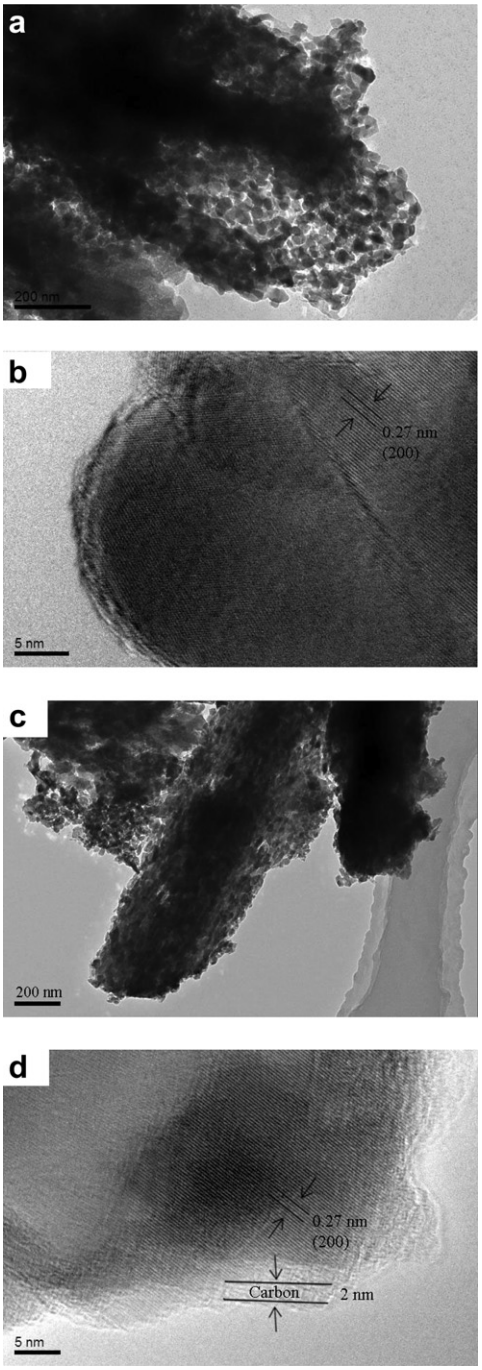

Fig. 4. TEM images of (a, b) FeS_2 and (c, d) FeS_2/C particles.

and Li_xPF_y. The ratio of LiF peak area of FeS_2 electrode to that of the FeS_2/C electrode is about 25:18, indicating the reduced amounts of LiF in FeS_2/C. It is no doubt attributed to the carbon coating, which reduces HF corrosion, and thus improves the electrochemical performances of the cells.

The XRD patterns of the FeS_2 and FeS_2/C electrodes charged to 2.6 V after 50 cycles are shown in Fig. 8. The broad diffraction peak from 14 to 25° in 2θ degree comes from the PVC film. The peak of Al is attributed to the Al current collector (the reaction product is scraped off the current collector). For the FeS_2 electrode, besides the peak of Al, other peaks are indexed to S, FeS, Li_2FeS_2 and Li_2S. It is supposed that the reaction transforming from Li_2S and Fe to Li_2FeS_2 is not complete, thus Li_2S is detected even if some Li_2S is

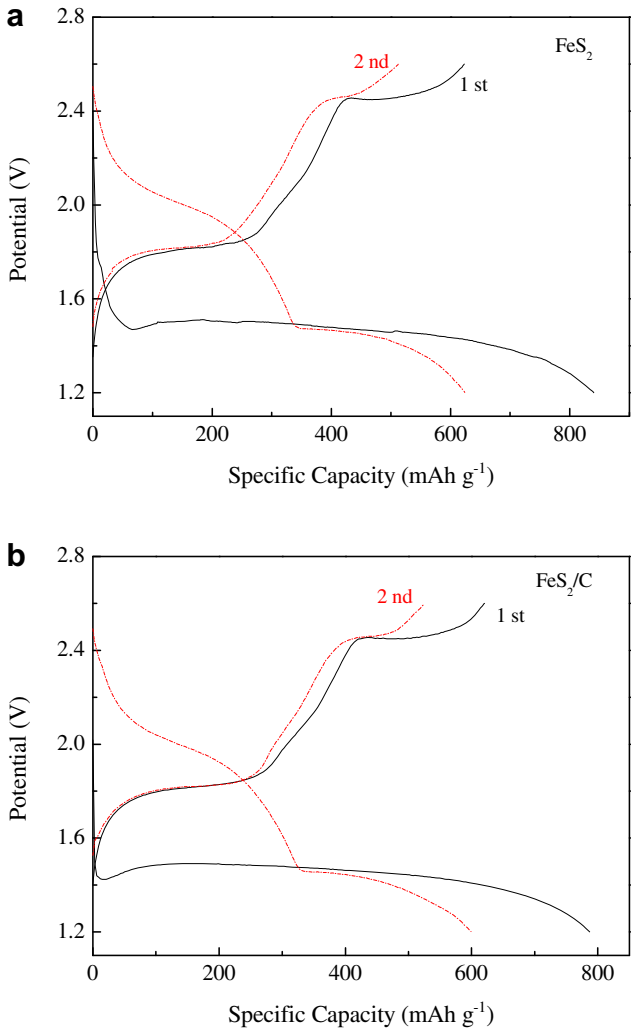

Fig. 5. Discharge–charge curves of (a) FeS_2 and (b) FeS_2/C electrodes between 1.2 and 2.6 V at 0.05 C.

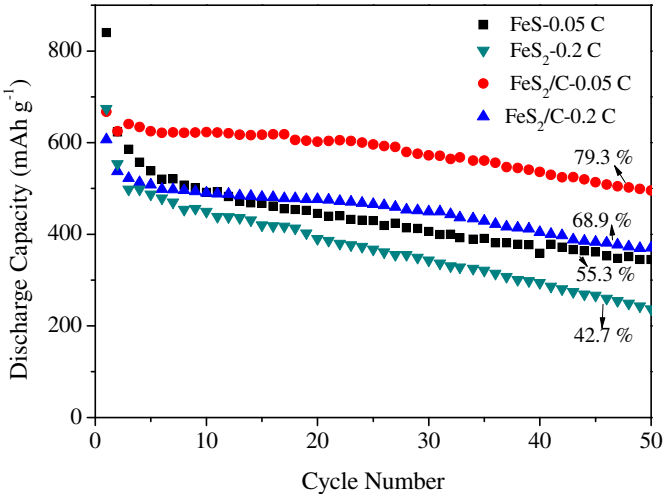

Fig. 6. Cycling performance of FeS_2 and FeS_2/C electrodes at 0.05 and 0.2 C between 1.2 and 2.6 V for 50 cycles.

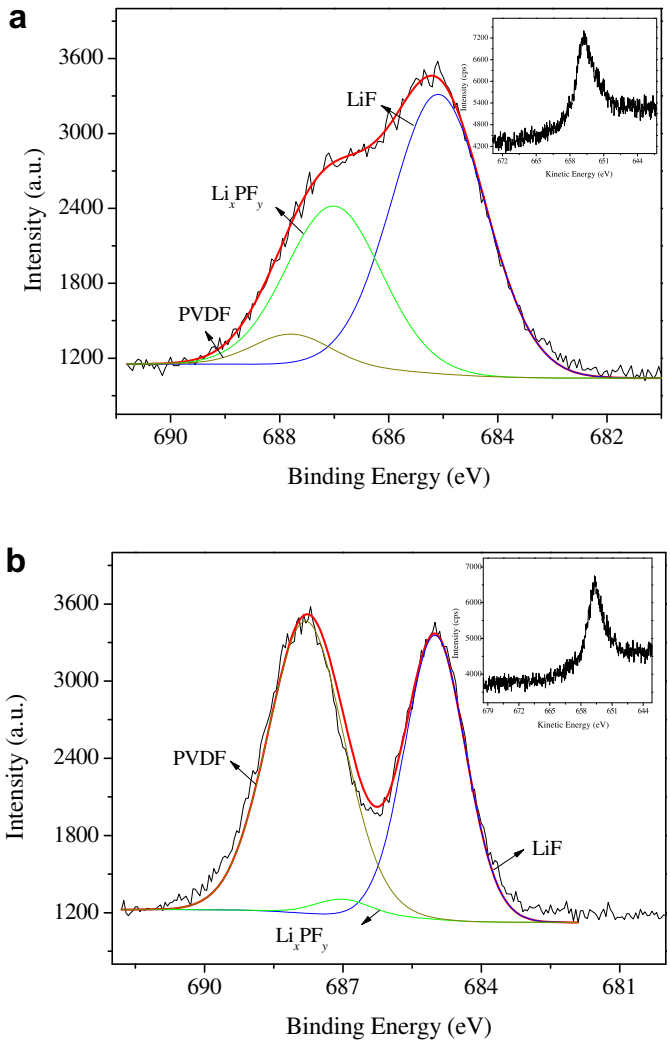

Fig. 7. XPS spectra of F 1s of (a) FeS_2 and (b) FeS_2/C electrodes (the inset is Auger spectrum).

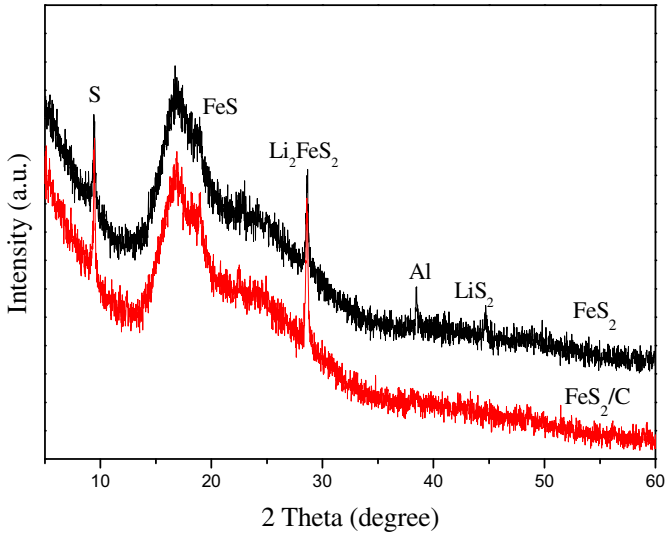

Fig. 8. XRD patterns of FeS_2 and FeS_2/C electrodes charged to 2.6 V after 50 cycles.

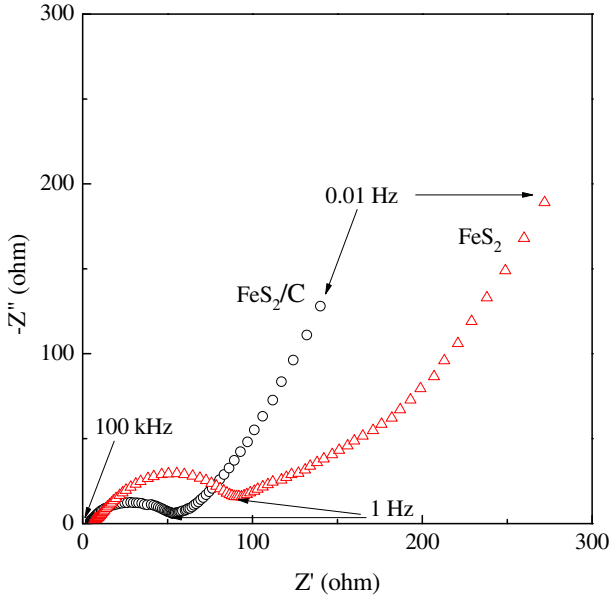

Fig. 9. Nyquist plots of FeS_2 and FeS_2/C electrodes at a discharge state after the 5th cycles in the frequency range of 100 kHz–0.1 Hz.

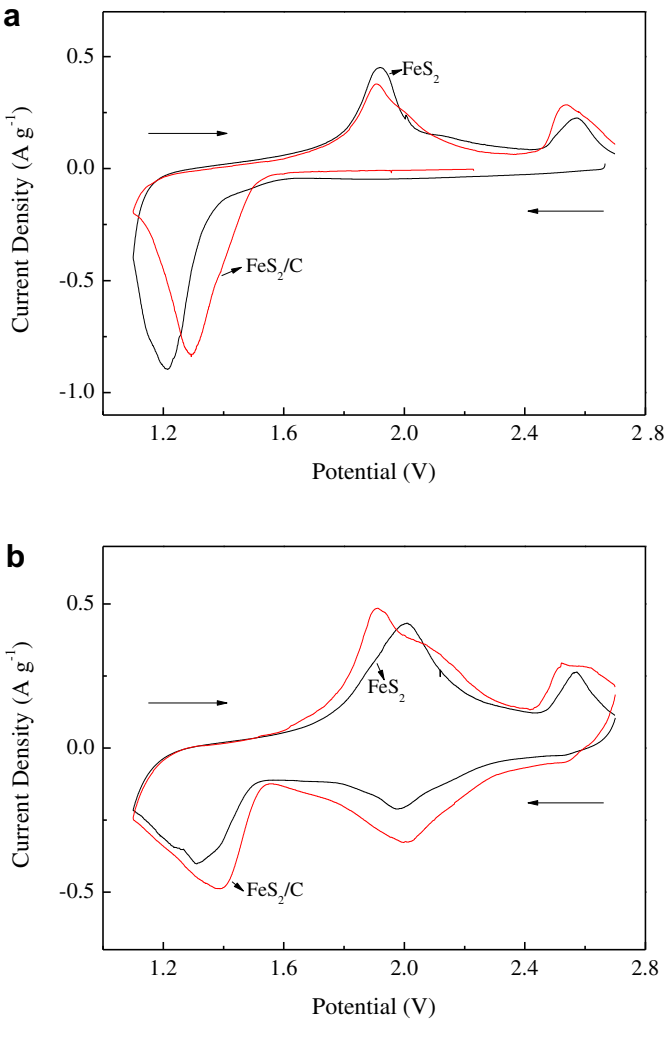

Fig. 10. CV curves of FeS_2 and FeS_2/C electrodes for (a) the first cycle and (b) the fifth cycle between 1.1 and 2.7 V (versus Li/Li$^+$) at a scan rate of 0.1 mV s^{-1}.

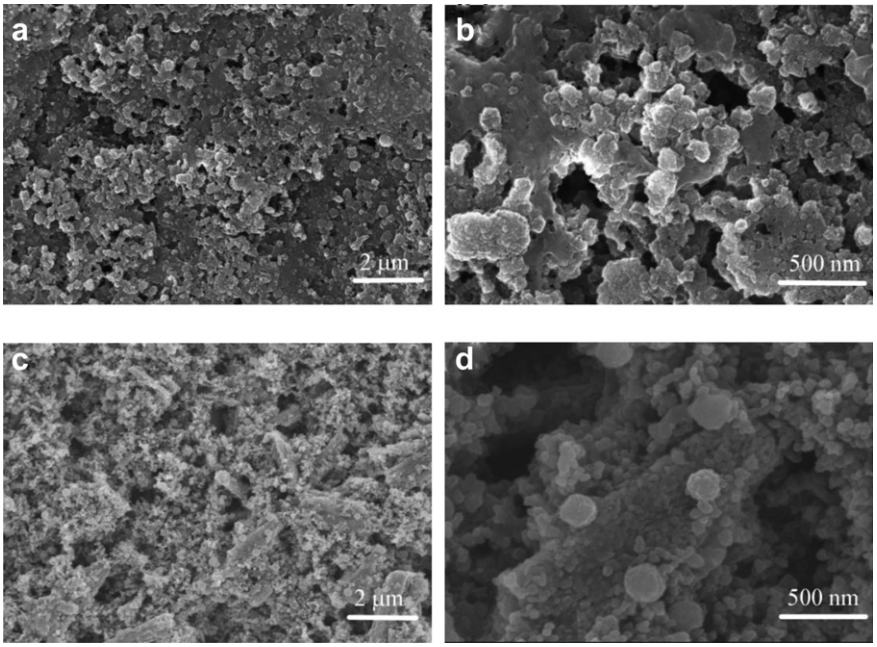

Fig. 11. SEM images of the (a, b) FeS_2 and (c, d) FeS_2/C electrodes after 50 cycles at 0.05 C.

consumed by HF. However, Li_2S is not observed in the FeS_2/C electrode, suggesting the more complete electrochemical reaction and the better reversibility of FeS_2/C composite. Besides, the intensity of Li_2FeS_2 for the FeS_2/C electrode is a little higher than that of the FeS_2, due to the more complete electrochemical reaction.

In addition, the result of ICP shows that the composition of the S in cycled electrolyte is 1.91 and 1.44 μg ml^{-1} for the FeS_2 and FeS_2/C electrodes, respectively. It is confirmed the protective effect of the carbon coating on reducing the dissolution of sulfur, which improves the cycling performance of FeS_2 electrode.

EIS analysis of electrodes after the 5th cycle discharged to 1.2 V is shown in Fig. 9. It is generally believed that the semicircle at middle frequency region is ascribed to the charge-transfer impedance at the electrode/electrolyte interface, while the line in the lower frequency region is corresponded to the diffusion of lithium ions within electrodes [41]. It is obviously shown that the diameter of the semicircle in medium-frequency region for the FeS_2/C electrode is smaller than that of FeS_2, indicating lower charge-transfer impedances. As is well known, the electrical conductivity is one of the main causes for the charge transfer resistance [42,43]. Therefore, it is concluded that the carbon coating supplies fast charge transfer channels on the interface of FeS_2/electrolyte.

The enhanced electrical conductivity of FeS_2/C electrode can also be confirmed by CV curves in Fig. 10. It exhibits a single reduction peak and two oxidation peaks in the first cycle, and two reduction peaks in the fifth cycle which are consistent well with the discharge-charge plateaus in Fig. 5. For the first cycle, the FeS_2 electrode exhibits high intensity of electrochemical peaks, suggesting the large amount of Li^+ react with FeS_2 in the discharge process. However, in the fifth cycle, the FeS_2 electrode exhibits the higher potentials of oxidation peaks and lower potentials of corresponding reduced peaks, indicating the large polarization for the lithium extraction/insertion process. The polarization is associated with the transferring delay of electrons on the active material/electrolyte interface [44]. The smaller polarization in the FeS_2/C electrode indicates the facilitated electron and ion transferring during electrochemical reactions.

Fig. 11 gives SEM images of the FeS_2 and FeS_2/C electrodes after 50 cycles at 0.05 C. It can be seen clearly that the original rod-like structure of FeS_2 disappears completely due to the drastic volume changes during discharge and charge process (Fig. 11a and b) [26]. Besides, a connected network-like structure appears which is caused by the aggregation of particles [45,46]. However, for the FeS_2/C electrodes, the rod-like porous structure keeps well, indicating that the porous FeS_2 is stabilized by the carbon (Fig. 11c and d). The carbon coating is considered to buffer the drastic volume change during discharge and charge process, keeping the porous structure of active material and improving the electrochemical performance [23,47].

4. Conclusions

FeS_2/C composite was synthesized using glucose as a carbon source via a simple solid state reaction. The carbon was coated on porous FeS_2 particle surface. Better cycling performance was obtained for the FeS_2/C electrode. The specific capacity of the FeS_2/C composite after 50 cycles is 495 mAh g^{-1}, much higher than that of FeS_2 (345 mAh g^{-1}). The improvements can be attributed to the carbon coating, which enhances the electrical conductivity, reduces dissolution of sulfur and corrosion from HF, and stabilizes the porous structure of active material during cycling.

Acknowledgments

The authors would like to acknowledge financial support from the Fundamental Research Funds for the Central Universities (2011QNA4006) and Key Science and Technology Innovation Team of Zhejiang Province (2010R50013).

References

[1] E. Strauss, G. Ardel, V. Livshits, L. Burstein, D. Golodnitsky, E. Peled, J. Power Sources 88 (2000) 206–218.
[2] E. Peled, D. Golodnitsky, E. Strauss, J. Lang, Y. Lavi, Electrochim. Acta 43 (1998) 1593–1599.
[3] S.Y. Huang, X.Y. Liu, Q.Y. Li, J. Chen, J. Alloy. Compd. 472 (2009) L9–L12.
[4] L.A. Montoro, J.M. Rosolen, Solid State Ionics 159 (2003) 233–240.
[5] Y.J. Choi, N.W. Kim, K.W. Kim, K.K. Cho, G.B. Cho, H.J. Ahn, J.H. Ahn, K.S. Ryu, H.B. Gu, J. Alloy. Compd. 485 (2009) 462–466.

[6] Z.S. Wen, J. Yang, B.F. Wang, K. Wang, Y. Liu, Electrochem. Commun. 5 (2003) 165–168.
[7] G.X. Wang, J.H. Ahn, J. Yao, S. Bewlay, H.K. Liu, Electrochem. Commun. 6 (2004) 689–692.
[8] G. Derrien, J. Hassoun, S. Panero, B. Scrosati, Adv. Mater. 19 (2007) 2336–2340.
[9] X.H. Huang, J.P. Tu, C.Q. Zhang, X.T. Chen, Y.F. Yuan, H.M. Wu, Electrochim. Acta 52 (2007) 4177–4181.
[10] J.Y. Xiang, J.P. Tu, J. Zhang, J. Zhong, J.P. Cheng, Electrochem. Commun. 12 (2010) 1103–1107.
[11] L.B. Chen, X.M. Yin, L. Mei, C.C. Li, D.N. Lei, M. Zhang, Q.H. Li, Z. Xu, C.M. Xu, T.H. Wang, Nanotechnology 23 (2012) 035402.
[12] Y. Lu, J.P. Tu, J.Y. Xiang, X.L. Wang, S.X. Mao, J. Mater. Chem. 21 (2011) 17988–17997.
[13] J. Saint, M. Morcrette, D. Larcher, L. Laffont, S. Beattie, J.P. Peres, D. Talaga, M. Couzi, J.M. Tarascon, Adv. Funct. Mater. 17 (2007) 1765–1774.
[14] L.Q. Tao, J.T. Zai, K.X. Wang, H.J. Zhang, M. Xu, J. Shen, Y.Z. Su, X.F. Qian, J. Power Sources 202 (2012) 230–235.
[15] K. Chang, Z. Wang, G.C. Huang, H. Li, W.X. Chen, J.Y. Lee, J. Power Sources 201 (2012) 259–266.
[16] Y.J. Mai, S.J. Shi, D. Zhang, Y. Lu, C.D. Gu, J.P. Tu, J. Power Sources 204 (2012) 155–161.
[17] N. Jayaprakash, W.D. Jones, S.S. Moganty, L.A. Archer, J. Power Sources 200 (2012) 53–58.
[18] Z. Chen, Y. Qin, K. Amine, Y.K. Sun, J. Mater. Chem. 20 (2010) 7606–7612.
[19] R. Dominko, M. Bele, M. Gaberscek, M. Remskar, D. Hanzel, J.M. Goupil, S. Pejovnik, J. Jamnik, J. Power Sources 153 (2006) 274–280.
[20] F. Yu, J.J. Zhang, Y.F. Yang, G.Z. Song, J. Power Sources 189 (2009) 794–797.
[21] R. Dominko, M. Bele, J.M. Goupil, M. Gaberscek, D. Hanzel, I. Arcon, J. Jamnik, Chem. Mater. 19 (2007) 2960–2969.
[22] F. Yu, J.J. Zhang, Y.F. Yang, G.Z. Song, J. Power Sources 195 (2010) 6873–6878.
[23] Y. Zhu, Y.J. Bai, F.D. Han, Y.X. Qi, N. Lun, B. Yao, J.X. Zhang, Mater. Lett. 65 (2011) 3157–3159.
[24] J. Read, D. Foster, J. Wolfenstine, W. Behl, J. Power Sources 96 (2001) 277–281.
[25] X.H. Huang, J.P. Tu, C.Q. Zhang, J.Y. Xiang, Electrochem. Commun. 9 (2007) 1180–1184.
[26] D. Zhang, J.P. Tu, J.Y. Xiang, Y.Q. Qiao, X.H. Xia, X.L. Wang, C.D. Gu, Electrochim. Acta 56 (2011) 9980–9985.
[27] X. Sun, Y. Li, Angew. Chem. Int. Ed. 116 (2004) 607–611.
[28] R. Fong, J.R. Dahn, C.H.W. Jones, J. Electrochem. Soc. 136 (1989) 3206–3210.
[29] H.S. Kim, M. Kong, K. Kim, I.J. Kim, H.B. Gu, J. Power Sources 171 (2007) 917–921.
[30] J.T. Lee, F.M. Wang, C.S. Cheng, C.C. Li, C.H. Lin, Electrochim. Acta 55 (2010) 4002–4006.
[31] B. Markovsky, A. Rodkin, G. Salitra, Y. Talyosef, D. Aurbach, H.J. Kim, J. Electrochem. Soc. 151 (2004) A1068–A1076.
[32] R. Ruffo, S.S. Hong, C.K. Chan, R.A. Huggins, Y. Cui, J. Phys. Chem. C 113 (2009) 11390–11398.
[33] P. Velasquez, D. Leinen, J. Pascual, J.R. Ramos-Barrado, P. Grez, H. Gomez, R. Schrebler, R. Del Rio, R. Cordova, J. Phys. Chem. B 109 (2005) 4977–4988.
[34] E. Strauss, D. Golodnitsky, E. Peled, Electrochim. Acta 45 (2000) 1519–1525.
[35] M. Valli, I. Persson, Colloids Surf. A 83 (1994) 207–217.
[36] E. Strauss, D. Golodnitsky, K. Freedman, A. Milner, E. Peled, J. Power Sources 115 (2003) 323–331.
[37] D. Aurbach, J. Power Sources 89 (2000) 206–218.
[38] K. Edström, T. Gustafsson, J.O. Thomas, Electrochim. Acta 50 (2004) 397–403.
[39] J.M. Zheng, J. Li, Z.R. Zhang, X.J. Guo, Y. Yang, Solid State Ionics 179 (2008) 1794–1799.
[40] H. Yang, G.V. Zhuang, P.N. Ross Jr., J. Power Sources 161 (2006) 573–579.
[41] Y. Liu, X. Li, H. Guo, Z. Wang, W. Peng, Y. Yang, R. Liang, J. Power Sources 184 (2008) 522–526.
[42] J.Y. Xiang, J.P. Tu, L. Zhang, X.L. Wang, Y. Zhou, Y.Q. Qiao, Y. Lu, J. Power Sources 195 (2010) 8331–8335.
[43] X.H. Huang, J.P. Tu, X.H. Xia, X.L. Wang, J.Y. Xiang, Electrochem. Commun. 10 (2008) 1288–1290.
[44] D. Aurbach, B. Markovsky, I. Weissman, E. Levi, Y. Ein-Eli, Electrochim. Acta 45 (1999) 67–86.
[45] H. Li, L.H. Shi, Q. Wang, L.Q. Chen, X.J. Huang, Solid State Ionics 148 (2002) 247–258.
[46] Y.G. Guo, J.S. Hu, L.J. Wan, Adv. Mater. 20 (2008) 2878–2887.
[47] Y. Yao, J.J. Zhang, L.G. Xue, T. Huang, A.S. Yu, J. Power Sources 196 (2011) 10240–10243.